Assessment of imaging performance for metal alloys of the first Italian neutron imaging beamline NICHE (Pavia, Italy)

Journal of Instrumentation

SISSA

PAPER • OPEN ACCESS

Assessment of imaging performance for metal alloys of the first Italian neutron imaging beamline NICHE (Pavia, Italy)

To cite this article: L. Vigorelli *et al* 2024 *JINST* **19** C10003

Published by IOP Publishing for Sissa Medialab

Received: *July 1, 2024*
Accepted: *September 30, 2024*
Published: *October 16, 2024*

International Workshop on Imaging
Varenna (Lake Como), Italy
26–29 September 2023

Assessment of imaging performance for metal alloys of the first Italian neutron imaging beamline NICHE (Pavia, Italy)

L. Vigorelli,[a,b,*] **G. Marcucci**,[a,c] **D. Di Martino**,[a] **M. Clemenza**,[a] **F. Grazzi**,[d,e] **F. Cantini**,[d,e,f] **N. Gelli**,[e] **L. Giuntini**,[e,f] **F. Taccetti**,[e] **T.E. Bella**,[g] **O. Sans Planell**,[h,i] **M. Magalini**,[i] **A. Re**,[i] **L. Guidorzi**,[i] **M. Marabotto**,[i,b] **A. Lo Giudice**,[i] **A. Vietti**,[b] **S. Grassini**,[b] **M.P. Morigi**,[j] **M. Bettuzzi**,[j] **D. Alloni**,[k] **M. Prata**[k] **and A. Salvini**[k]

[a] *Dipartimento di Fisica "G. Occhialini", Università di Milano-Bicocca and INFN, Sezione di Milano-Bicocca, Milano, Italy*
[b] *Dipartimento di Scienze Applicate e Tecnologia, Politecnico di Torino and INFN, Sezione di Torino, Torino, Italy*
[c] *STFC ISIS Neutron and Muon Source, Didcot, United Kingdom*
[d] *Consiglio Nazionale delle Ricerche, Istituto di Fisica Applicata "Nello Carrara", Sesto Fiorentino, Italy*
[e] *INFN, Sezione di Firenze, Sesto Fiorentino, Italy*
[f] *Dipartimento di Fisica e Astronomia, Università di Firenze, Firenze, Italy*
[g] *Indipendent Researcher*
[h] *Helmholtz Centre Berlin for Materials and Energy, Berlin, Germany*
[i] *Dipartimento di Fisica, Università di Torino and INFN, Sezione di Torino, Torino, Italy*
[j] *Dipartimento di Fisica ed Astronomia "Augusto Righi", Università di Bologna and INFN, Sezione di Bologna, Bologna, Italy*
[k] *Laboratorio Energia Nucleare Applicata (LENA) and INFN, Sezione di Pavia, Pavia, Italy*

E-mail: luisa.vigorelli@unimib.it

Abstract: In this paper, the imaging capabilities and performance of the new neutron imaging beamline developed at the LENA facility of Pavia (Italy) in the framework of the NICHE project (Neutron Imaging in Cultural HEritage) are presented. For this purpose, the estimation of bronze and brass alloys attenuation coefficient has been obtained through imaging analysis of a set of Cu-based alloy reference samples produced ad-hoc with chemical composition similar to ancient artefacts. In addition, some samples were realised using a different cooling ramp in order to test the influence of the alloy production procedures in neutron attenuation. Moreover, the tomographic capabilities of the beamline were tested for different metallic and plastic materials.

Keywords: Data analysis; Image processing; Neutron radiography

*Corresponding author.

https://doi.org/10.1088/1748-0221/19/10/C10003

2024 JINST 19 C10003

Contents

2024 JINST 19 C10003

1 Introduction

In the context of the research with neutron imaging techniques, the "NICHE" project (Neutron Imaging for Cultural HEritage) promoted by the Cultural Heritage Network (CHNet) of the Istituto Nazionale di Fisica Nucleare (INFN) was devoted to the development of a new station for neutron imaging analysis specifically dedicated to the study of Cultural Heritage objects [1] at the Laboratorio Energia Nucleare Applicata (LENA) in Pavia (Italy). For this purpose, five Italian INFN sections (Firenze, Milano Bicocca, Bologna, Torino, and Pavia) were involved. The NICHE beamline was installed on the thermal port of the 250 kW TRIGA Mark-II reactor managed by the LENA [2] and its development consisted of several steps, starting from the design and construction of different instrumentation components [3, 4] and proceeding with several tests conducted to characterise the instrumentation and verify the performance of the beamline [4]. Among them, beamline calibration was carried out using purposely prepared specimens, with a known composition, to estimate the empirical neutron attenuation coefficient for different materials. Several samples of copper-based metal alloys with ligand elements at different concentrations were produced to simulate ancient metallic materials. In this context, the attenuation coefficient as a function of the alloy composition was evaluated.

2 Materials and methods

A set of Cu-based reference alloys, 4 mm thick disks cut from different ingots (Cu-Sn, Cu-Zn and Cu-Sn-Pb alloys), similar to the expected composition of bronze and brass ancient artefacts, were produced in the laboratory, according to a standardized protocol [5]. Binary alloys were prepared with different concentrations of tin and zinc in the range of 4–12wt% and 5–25wt%, respectively; the ternary alloy with lead, was made with a fixed amount of tin (6wt%) and increasing the Pb concentration in the range of 4–16wt%. All the samples were then analysed by means of Optical Emission Spectroscopy (OES) to quantify the chemical composition, together with a pure copper reference sample (table 1 and table A in the supplementary data). In addition to these reference sample set, three step wedges (150 mm long) made of steel, brass and bronze were also analysed [6]. Furthermore, a composite sample made of an aluminium cylinder with eccentric holes filled with rods of different materials (brass, polyethylene, iron, copper, silver, lead and aluminium) was analysed by means of neutron tomography [7]. Concerning the analysis, the most suitable experimental configuration and data treatment was adopted, as determined from previous instrument characterisation [4, 5]. For each different alloy composition, two flat disk shape samples with similar thickness were analysed (labelled

A and B) measuring transmittance; the disks were also analysed together overlapping, to obtain a single sample of double thickness (in some cases, a third disk was available, and it was also possible to analyse the triple thickness). The sample holder, made in aluminium, was mounted on the sample manipulation stage to carry out automatic movements along the horizontal and vertical directions. In this way it was possible to move different set of samples in and out of the beam (65 mm diameter field of view) to obtain images for all the samples mounted on the support (figure A in the supplementary data). In addition, open beam (beam measurement without the object) and dark current (electronic noise without beam) images were acquired for image processing and normalisation. After images were pre-processed to remove "white-spots", i.e., outliers caused, among others, by γ rays directly hitting the detector CMOS chip, data were normalised by dark subtraction and flat-field normalisation. A single squared region of interest (ROI) of 50×50 pixel in the central area of each sample was selected to obtain the transmission intensity value in the normalised images, then the attenuation coefficient Σ was calculated according to the Lambert-Beer exponential law $I = I_0 e^{-\Sigma d}$, where d is the thickness of the sample. In this case, both the absorption and scattering cross section contribute to total attenuation.

Table 1. Samples elements concentrations (wt%) obtained with OES measurements.

Binary bronzes (Cu-Sn)	*Ternary bronzes (Cu-Sn-Pb)*	*Brasses (Cu-Zn)*
B08(Sn4): 95-5%	C3(Pb4): 89-6-5%	Zn5: 95-5%
B09(Sn6): 93.5-6.5%	C7(Pb4): 89-5-6%	Zn10: 91-9%
B10(Sn9): 90-10%	C8(Pb4): 88-5-7%	Zn15: 86-14%
B11(Sn12): 89-11%	C4(Pb8): 84-6-10%	Zn20: 82-18%
R-Sn9: 92-8%	C5(Pb8): 83-6-11%	Zn25: 79-21%
R-Sn12: 90%-10%	C11(Pb12): 80-6-14%	
	C6(Pb16): 74-5-21%	
	R-Pb8: 84-6-10%	
	R-Pb12: 76-5-19%	

3 Results

Binary and ternary alloys. From the obtained results, a difference of the attenuation coefficients of bronze and brass binary alloys samples compared to pure copper is visible from graphs in figure 1a-c. Despite the decrease of the attenuation values with respect to pure copper specimens, no substantial differences between samples with different Sn% and Zn% concentrations can be appreciated, as expected instead with the increase of tin and zinc from theoretical calculation [8] (except for the ternary alloys with Pb, where a slightly decrease of the attenuation coefficient with the increase of lead concentration can be noticed). This is very likely due to specific characteristics of the samples and the preparation method. A possible explanation for this behaviour is the fact that all the samples observed in neutron radiography produce some bright spots all around them, showing a typical scattering signal induced by the presence of ordered macro-crystals [9]. This effect is much stronger than the attenuation law induced by absorption and scattering from a powder-like polycrystalline sample. Evidence of this effect is visible in several full normalised images, varying brightness and contrast, especially in the parts of the acquisition window that are out of the transmitted neutron beam projected in the circular

2024 JINST 19 C10003

field of view (figure 1d). Neutron scattering is related to the crystalline microstructure of the samples, which in turn is linked to the cooling method of the alloy. In our case, the formation of macro-crystals, with also some dendrites, visible in the metallographic analysis (figure B in supplementary data), became the main attenuation source thus influencing the overall attenuation power of the samples and showing a behaviour that is independent from the ligand amount and type. To mitigate this effect and check possible differences in attenuation coefficients, a small set of Cu-Sn and Cu-Sn-Pb samples was made with a different cooling ramp after melting (a step cooling ramp, figure C in the supplementary data) where every 200 °C the temperature was maintained constant for 1 hour. Comparing the results obtained from samples with similar final composition but made with the two different cooling ramps, no significant differences between the attenuation coefficients can be appreciated (figure 1e), then it is possible to infer that no changes in the formation of the macro-crystals was obtained (attenuation coefficients values are reported in table B in the supplementary data).

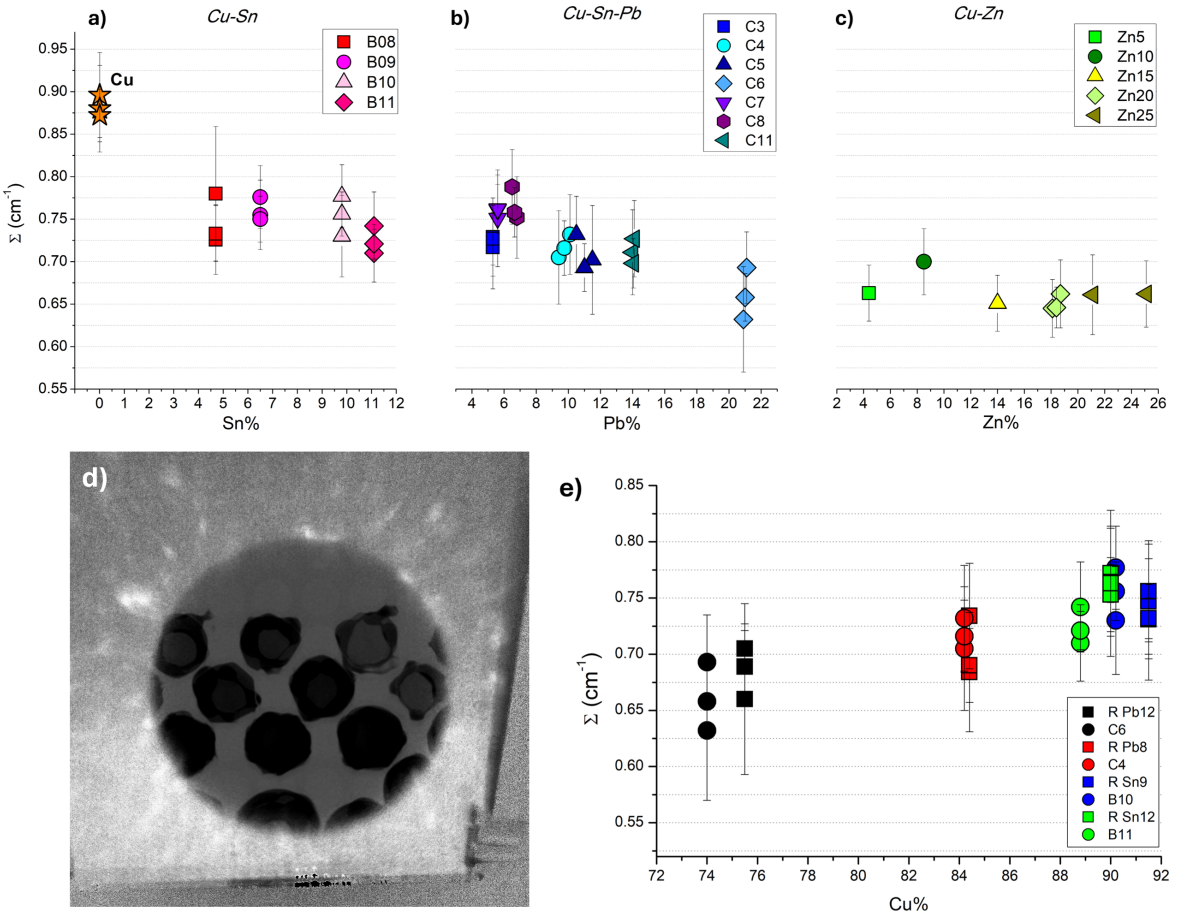

Figure 1. Attenuation coefficient values calculated for a) Cu-Sn, b) Cu-Sn-Pb and c) C-Zn samples; d) effect of sample scattering visible as bright spots in and out of the field of view (round area in the centre) in the full normalised image; e) comparison of samples made with the two different cooling ramp (R-samples are the ones produced with the step cooling ramp; same colour refers to compared samples).

2024 JINST 19 C10003

Step wedge. Each step of the wedges is a 10×10 mm^2 square with an increasing thickness of 2 mm per step, up to a maximum of 30 mm. Figure 2a shows the radiographic image of the three step wedges and the corresponding grey level profiles, where a decrease of the transmission value with the increase of the thickness of each step (right to left in the figure) can be appreciated, up to the largest thickness where the noise contribution starts to dominate. Differences in the neutron transmission (and therefore in the attenuation coefficient) for the different wedge materials are observable in the separation among the three profiles. Attenuation coefficients were obtained from the exponential fit performed plotting the I/I_0 values as a function of step thickness, in which a limit value for the decay related to scattering is considered (figure 2b). Stronger scatterers as iron show a higher value for the high thickness plateau.

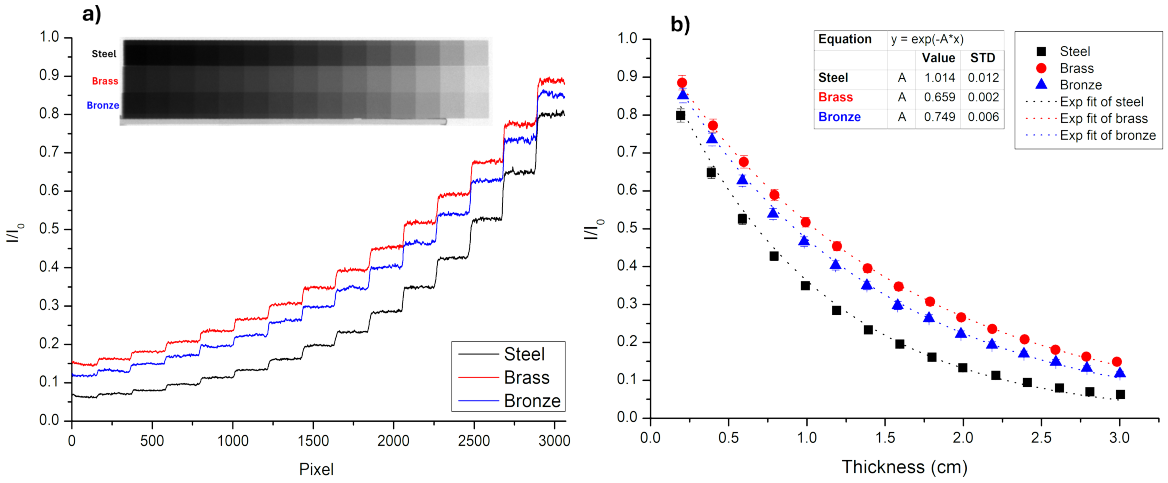

Figure 2. a) Radiography and transmission profile of the three step wedges; b) neutron attenuation curves for the three wedges as a function of the step thickness.

Cylinder sample CT. The different metallic cylinders were positioned into the holes of the aluminium cylinder, as in the scheme shown in figure 3a. The sample was rotated by angular steps of 1.2° up to 360°, obtaining 300 projections with an exposure time of 150 s for each projection. The CT reconstruction, corrections and data analysis were performed using the Python NeuTomPy Toolbox library [10], a powerful open-source code developed to process neutron tomographic data, and the ImageJ software [11]. The reconstruction was performed with a GPU-based iterative algorithm, after some pre-processing filtering steps to suppress outliers and ring artifacts. In the reconstructed slice in figure 3b it is possible to observe that attenuation coefficients of the various elements are significantly different (distinguishable also in the slice histogram, figure 3c) and each cylinder volume can be easily segmented (figure D in the supplementary data). The slices containing the polyethylene cylinder (PE) are affected by strong noise artefacts due to the high incoherent scattering events induced by the hydrogen content, visible also in the 3D rendering (figure D in the supplementary data).

Moreover, polyethylene and silver cylinders show differentiated attenuation in their own volume, due to the beam hardening effect. Applying specific corrections, different for the two materials (polynomial on the single volumes), it is possible to reduce the beam hardening effect, as shown in figure 4. The obtained attenuation coefficients are listed in table C in the supplementary data.

2024 JINST 19 C10003

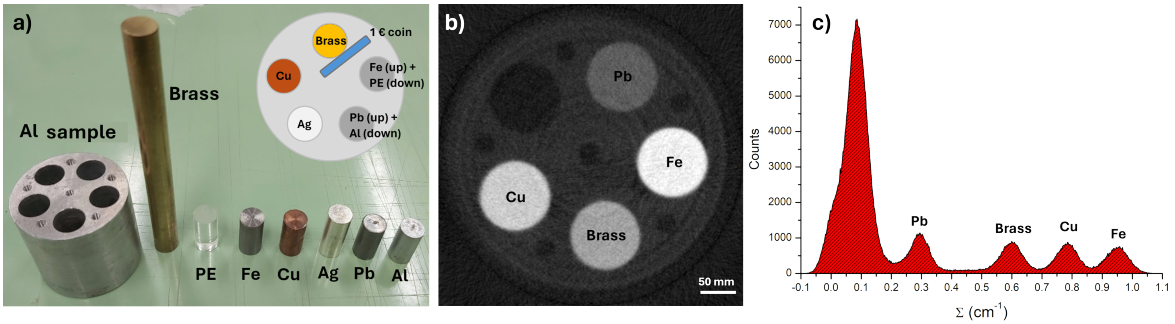

Figure 3. a) The Al sample with the analysed cylinders and positions scheme; b) reconstructed slice in which the different cylinders are clearly distinguishable; c) histogram of the slice in which the separated peaks refer to different materials (the highest one is related to the background and the Al sample holder).

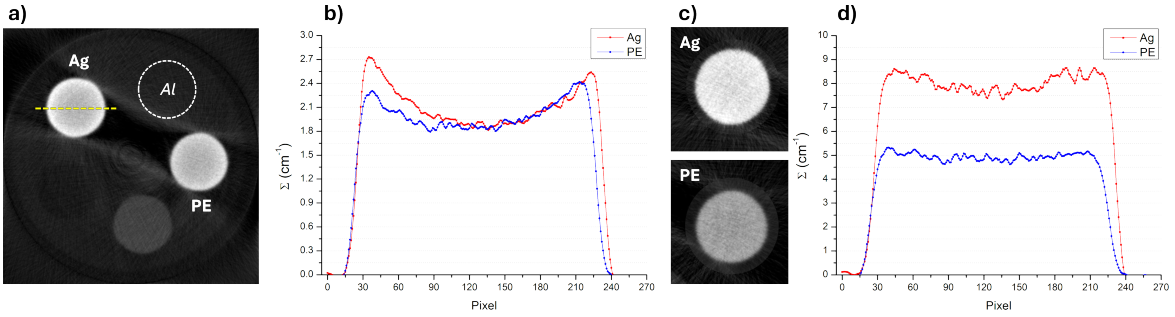

Figure 4. Reconstructed slice with Ag and PE cylinders (Al one is not visible) without (a) and with (c) beam hardening correction, with the correspondent profile (along yellow line for all the samples) in b) and d) respectively. As can be noticed, attenuation coefficient increases when beam hardening correction is applied.

4 Conclusion

A series of measurements were performed to characterise the capabilities of the new NICHE imaging beamline for the analysis of different metal alloys samples. For this purpose, bronze and brass samples with different elements concentrations were prepared and analysed, to estimate attenuation coefficients as a function of Cu, Sn, Pb and Zn relative concentrations. The production procedure resulted in the formation of several large size crystals, that strongly affected the transmittance measurement. Tomographic capabilities were also tested with a multi-materic (metals and plastic) sample. It should be considered that the estimated total attenuation coefficient includes both absorption and scattering components. In this sense, scattering events can depend on sample microstructure (but also on multiple scattering and scattering from the bulk material, even if these aspects have not been taken into account in this case) and can differently influence the quantitative evaluation of neutron imaging results, as we experienced in our data. This is due to the fact that large coherent bunches of scattered neutrons could reach the detector almost everywhere and be counted as a transmitted signal, leading to incorrect estimation of the attenuation coefficients with respect to isotropic powder-like samples. The production method of the alloy specimens then has a fundamental role for quantitative analysis and beamline calibration purposes, starting from the powder materials. However, a more in-depth study and further tests for scattering correction and simulation of attenuation coefficients based on the facility characteristic should be performed. The determination of the attenuation coefficients

2024 JINST 19 C10003

of metal alloys is an important step towards the use of a neutron imaging beamline as a reliable non-invasive evaluation method in different fields of application, including Cultural Heritage. From the attenuation coefficients, measurement specifications needed according to experimental setup, sample size, condition, etc. can be derived for future experiments.

Acknowledgments

The INFN V committee, the INFN-CHNet network and the whole CHNet-NICHE collaboration are gratefully acknowledged for the support to the development of this activity.

References

[1] N. Kardjilov and G. Festa eds., *Neutron methods for archaeology and cultural heritage*, Springer (2017) [DOI:10.1007/978-3-319-33163-8].

[2] https://lena.unipv.it/wp-content/uploads/2020/03/50mo-LENA-web.pdf.

[3] N. Gelli et al., *The new INFN-CHNet neutron imaging facility*, *Nucl. Instrum. Meth. A* **1051** (2023) 168189.

[4] F. Grazzi et al., *A work-horse neutron imaging station at the Laboratorio Energia Nucleare Applicata (LENA) in Pavia (Italy): Instrumental components and applications in the frame of the CHNet-NICHE INFN experiment*, *J. Phys. Conf. Ser.* **2605** (2023) 012006.

[5] A. Vietti et al., *Realisation and characterisation of Cu based references for neutron imaging calibration purposes and first results*, *Acta IMEKO* **12** (2023) 1.

[6] E.A. Durisi et al., *Characterization of a neutron imaging setup at the INES facility*, *Nucl. Instrum. Meth. A* **726** (2013) 31.

[7] A.P. Kaestner et al., *Verifying Neutron Tomography Performance using Test Objects*, *Phys. Procedia* **43** (2013) 128.

[8] https://www.ncnr.nist.gov/resources/n-lengths/.

[9] S. Peetermans et al., *Simultaneous neutron transmission and diffraction imaging investigations of single crystal nickel-based superalloy turbine blades*, *NDT & E Int.* **79** (2016) 109.

[10] D. Micieli, T. Minniti and G. Gorini, *NeuTomPy toolbox, a Python package for tomographic data processing and reconstruction*, *SoftwareX* **9** (2019) 260.

[11] M.D. Abràmoff et al., *Image Processing with ImageJ*, *Biophotonics Int.* **11** (2004) 36.

2024 JINST 19 C10003